Forest Ecology and Management 612 (2026) 123704

Contents lists available at ScienceDirect

Forest Ecology and Management

journal homepage: www.elsevier.com/locate/foreco

A stochastic forest simulator accurately describes variation in boreal forest structure across Quebec, Canada

Rebecca Banbury Morgan [a,b,*], Timothy Baker [a], Louis Duchesne [c], Emmanuel Gloor [a], Roel Brienen [a]

[a] School of Geography, University of Leeds, Seminary St, Woodhouse, Leeds LS2 9JT, UK
[b] School of Biological Sciences, University of Bristol, 24 Tyndall Avenue, Bristol BS8 1TQ, UK
[c] Direction de la recherche forestière, ministère des Ressources naturelles et des Forêts du Québec, 2700 Einstein, Québec, Québec G1P 3W8, Canada

ARTICLE INFO

Keywords:
Forest modelling
Boreal forest
Mortality
Growth simulation
Forest structure

ABSTRACT

Improving our understanding of the dynamic links between demographic rates and forest structure is essential for accurately modelling forest responses to global change. Although individual-based modelling approaches offer a valuable means of gaining insights into the effects of growth and mortality on forest size and age structures, most require detailed physiological data that are not readily available. Here, building on previously developed stochastic growth simulations for single species, we simulate multi-species forest age and stem diameter distributions using stem diameter growth and mortality data from the Quebec provincial forest inventory program. The simulator accurately reproduces forest size and age structures derived from forest inventory and tree ring data and successfully replicates the variation in forest structure among different forest types and across latitudes. In contrast to most individual-based models, this approach does not require complex parameterization of growth functions. We anticipate that this method will have a wide range of applications in exploring the links between demographic rates, forest size and age structure, stem turnover rates, and biomass across forests globally, and by extension improve our understanding of forest dynamics in a changing world.

1. Introduction

Forests hold a large proportion of terrestrial biomass and are an important component of the global carbon cycle (Friedlingstein et al., 2022; Pan et al., 2024). Understanding forest responses to environmental change is thus a high research priority. In particular, improving our knowledge of how demographic rates affect forest structure and dynamics is essential for predicting forest responses to global atmospheric and climatic changes. Forest stand structure, the frequency distribution of stems across size classes, is important in determining aboveground biomass (Baraloto et al., 2011) and is shaped by variation in recruitment, growth, and mortality (Caspersen et al., 2011; Coomes and Allen, 2007; Muller-Landau et al., 2006).

Individual-based models link information on demographic rates, species traits, and responses to disturbance and environmental variables with whole-forest outcomes, and therefore offer a way to explore relationships between demography and stand structure (Fortin et al., 2009; Fortin and Langevin, 2012; Fischer et al., 2016; Hember and Kurz, 2018; Pacala et al., 1996). These models are typically built around processes of forest dynamics, including gap formation (Fischer et al., 2016; Pacala et al., 1996) and competition (Chave, 1999), which are determined by tree physiology or resource use (Rammer et al., 2024). Although these models can generate accurate projections of forest dynamics, they are often data-intensive to parameterize, which limits their application in testing how simple demographic processes affect forest structure.

Simple phenomenological approaches, such as stochastic growth simulations (Lieberman et al., 1985; Lieberman and Lieberman, 1985; Cruz et al., 2020) may enable more direct analysis of the effect of demographic rates on forest structure. Stochastic growth simulations sample diameter growth increment data from forest inventory data to generate trajectories of individual stem growth (Lieberman et al., 1985; Lieberman and Lieberman, 1985). The original approach randomly sampled growth data from trees of similar diameter and was subsequently extended to sample single-species tree ring data (Brienen et al., 2006). However, this approach could also be applied to multi-year forest

* Corresponding author at: School of Geography, University of Leeds, Seminary St, Woodhouse, Leeds LS2 9JT, UK.
E-mail addresses: becky.banburymorgan@bristol.ac.uk (R. Banbury Morgan), t.r.baker@leeds.ac.uk (T. Baker), louis.duchesne@mrnf.gouv.qc.ca (L. Duchesne), e.gloor@leeds.ac.uk (E. Gloor), r.brienen@leeds.ac.uk (R. Brienen).

https://doi.org/10.1016/j.foreco.2026.123704
Received 12 November 2025; Received in revised form 12 March 2026; Accepted 14 March 2026
Available online 27 March 2026

inventory data from natural forest stands (e.g., Anderson-Teixeira et al., 2015; ForestPlots.net et al., 2021; Gray et al., 2012). Because the effects of stem size and previous growth rate are accounted for in the sampling approach, rather than by development of specific growth functions, this approach has great potential to be developed into a flexible, data-driven approach to simulating stand and age structures that can be applied across datasets and forest ecosystems.

Here, we integrate forest inventory and tree ring data from the permanent sample plots network of the Quebec provincial forest inventory program (Ministère des Forêts, de la Faune et des Parcs MFFP, 2016; Ministère des Ressources naturelles et des Forêts MRNF, 2022) to extend the methods developed by Brienen et al. (2006) for simulating individual tree growth trajectories, and build (using short-term growth and mortality data from forest inventories) and validate (using size and age data from tree rings and inventories) a full individual-based simulation of forest structure. The simulation approach provides a "null" model of forest dynamics, which can be used to explore how changes in growth and mortality influence forest size and age structures, and to extend our understanding of forest structural responses to changes in demographic rates.

The Quebec provincial forest inventory program is a unique dataset, containing both forest census data and randomly sampled tree ring data surveyed from across the same set of inventory plots. This enables us to scale up the approach from simulation of single-species growth trajectories, to simulate and validate trajectories for multi-species forests and estimate stem diameter and age distributions. First, we test methods of simulating diameter growth trajectories by repeated sampling of growth increment data, and use tree ring data to validate that the method accurately simulates trajectories for multi-species forest stands. Second, we use simulated trajectories as a basis for modelling full stand structure and explore the influence of different approaches to estimating mortality on simulation outputs. We validate the simulated stem diameter distributions, lifetime growth rates, and stem age distributions across four ecological regions using a combination of forest inventory and tree ring data. Our results show that the method can accurately simulate variation in forest size and age structure across a large environmental gradient using forest inventory data on stem diameter, annual stem diameter growth rates, species wood densities, and regional-level estimates of mortality rates.

2. Methods

2.1. Quebec provincial forest inventory program datasets

We used data from the permanent sample plot network of the Quebec provincial forest inventory program (Ministère des Forêts, de la Faune et des Parcs MFFP, 2014, 2016; Ministère des Ressources naturelles et des Forêts MRNF, 2022), which covers four bioclimatic domains, defined based on climate and vegetation composition (Table 1; Figure S1). There are two temperate domains: the sugar maple-yellow birch domain, which consists mainly of deciduous forests dominated by sugar maple (*Acer saccharum* Marsh.), and the balsam fir-yellow birch domain, which is mainly mixed forests dominated by balsam fir (*Abies balsamea* (L.) Mill.). There are two closed-canopy boreal forest domains: the balsam fir-white birch domain, which is dominated by balsam fir; and the spruce-moss domain, which is dominated by black spruce (*Picea mariana* (Mill.) B. S. P.). The network comprises ~12000 permanent sampling plots at varying sampling intensities. All plots are circular with a radius of 11.28 m (0.04 ha in size), and have been resampled approximately every decade since the 1970s, with data from up to 6 censuses available. At each census, all trees with diameter at breast height (DBH) > 91 mm in the plot are measured and their species identity, DBH, and status (e.g. recruit, alive, or dead) is recorded. Mean census interval length is 11.8 years (range 3–35 years). Plots were excluded if they showed evidence of disturbance that had affected > 25% of the canopy (e.g. as a result of fire, clear cutting, severe insect outbreaks, or stand thinning interventions).

2.1.1. Inventory data processing

We used only forest inventory data to simulate growth trajectories and forest stand structure. For diameter growth trajectory simulations, only entries with stems alive in the census interval were selected from the plot dataset. Annual growth rates for each census interval were calculated by dividing census interval growth by census interval length. Due to measurement error, some growth increments were negative. We assumed errors of up to 10 mm between census measurements were reasonable but removed measurements where the measured DBH had declined by > 10 mm between censuses. Remaining negative growth increments were corrected to annual growth rates of 0 mm yr^{-1}. As this may introduce bias, we also ran simulations without correcting negative growth increments (Appendix A). Annual growth rates for the previous census interval were calculated for each stem at each census interval, and measurements without previous growth rates were excluded. We compiled a subset of annual growth data for recruits identified within the inventory dataset. All stems were assigned a species-specific wood density value extracted from the Global Wood Density Database (Chave et al., 2009), except for 1.7% of entries with unknown density which were removed.

2.1.2. Tree ring data processing

To validate the simulations, we used tree ring data compiled by the Quebec provincial forest inventory program. Since 1995, tree cores were sampled from permanent sample plots. In each plot, five randomly selected trees with a DBH > 91 mm were cored at 1 m above ground level. Cores were processed following standard procedure (dried, glued to a wooden tray, and sanded), so that ring boundaries could be detected

Table 1
Summary information for each bioclimatic domain, based on observed plot data, observed tree ring samples, and modelled mortality rates from plot census data.

Bioclimatic domain	Number of plots	Mean annual temperature (°C)	Number of species recorded in plots	Key species	Mean stem density (ha^{-1})	Mean basal area (m^2ha^{-1})	Mean stem DBH (mm)	Mean stem age (years)	Mean stem growth rate ($mmyr^{-1}$)	Mean stem mortality rate ($\%yr^{-1}$)
Sugar maple-yellow birch	2674	3	33	*Abies balsamea, Acer saccharum, Betula alleghaniensis*	795	26.2	183	33	2.9	4.7
Balsam fir-yellow birch	2923	2	24	*Abies balsamea, Betula alleghaniensis*	948	23.6	165	31	2.5	4.0
Balsam fir-white birch	2403	0.8	16	*Abies balsamea, Picea mariana, Betula papyrifera*	1079	20.7	148	26	2.2	4.0
Spruce-moss	2518	-1	10	*Picea mariana, Abies balsamea*	881	14.7	139	42	1.0	3.0

under magnification and measured using the WinDendro image analysis system to an accuracy of 0.01 mm. Tree growth trajectories were then compiled from annual growth steps. Quality control on core data was conducted to remove incomplete cores and to remove cores where significant differences between field-measured DBH and DBH calculated from tree rings were recorded.

While complete tree ring data are available for all 13 of the conifer species and the two most abundant shade-intolerant broadleaf species (*Betula papyrifera* Marsh. and *Populus* sp), data for other broadleaf species are missing. Tree ring data are available for species representing 59% of stems in the sugar maple-yellow birch domain; 85% of stems in the balsam fir-yellow birch domain; 99% of stems in the balsam fir-white birch domain; and all stems in the spruce-moss domain. Despite the discrepancies in species composition between the datasets, the stem diameter distributions of the tree ring samples are broadly representative of the stem diameter distributions observed from the plot data (Table S1, Figure S5).

2.2. Simulation specification

The simulation approach we develop here has two key components: 1) simulation of individual tree growth trajectories, and 2) repeated sampling of individual trajectories to simulate forest structure. All analyses were conducted by bioclimatic domain: inventory and tree ring data were aggregated at the domain level for building and validating the simulations, and we simulate domain-level parameters.

2.2.1. Growth trajectories

We used an approach similar to that in Brienen et al. (2006); (2012) to build age-diameter trajectories for individual stems. Trajectories were built by repeated sampling of growth rates from the inventory growth rate data (Fig. 1). We simulated a set of trajectories for each bioclimatic domain, using only inventory data for that domain. The starting DBH for each simulated tree was randomly sampled from the subset of recruits, and the trajectory initiated with the first 10 years of growth increments from the sampled stem.

Subsequent growth increments were generated by sampling annual growth rates from the full dataset. Growth increments vary over a stem's lifespan and may increase or decrease with increasing stem diameter (Anderson-Teixeira et al., 2022). Growth rates also vary among individuals and are generally positively correlated with previous stem growth rates (Brienen et al., 2006; Kohyama et al., 2005) and negatively with stem wood density (Chave et al., 2009). Accounting for both the size-dependency and autocorrelation in growth is essential to generate a realistic spread of growth rates within and between trajectories (Brienen et al., 2006). Here, autocorrelation includes both within-tree autocorrelation (i.e. temporal correlation of growth within single trees' growth series) as well as among-tree autocorrelation (i.e., persistent growth differences between trees, as per Brienen et al., 2006).

We tested five different approaches for building growth trajectories, in which the next growth increment was sampled according to different levels of autocorrelation. Growth increments were sampled from a subset of the database based on whether the characteristics of the stem fell within the following criteria::

1. The full stem dataset (the "basic" trajectories); or a subset of the dataset based on:
2. A diameter window, set as the current DBH of the simulated stem + /- 1%;
3. A growth rate window, set as the mean annual growth rate of the simulated stem over the preceding 10 years + /- 0.25 mm/yr;
4. A wood density window, set as the exact species-level wood density of the initial sampled stem; or
5. The combined effect of the above approaches, sampling according to growth rate, wood density, and diameter (Fig. 1)

Annual growth increment steps were added to the trajectory according to the length of the census interval in which the sampled growth increment was measured. This was repeated to generate a maximum of 300 growth steps (i.e. 300 years) for each simulated tree.

2.2.2. Mortality models

For each bioclimatic domain, we estimated mortality rates from the census data across all plots and censuses. Data for each stem at each census interval was included as a separate entry, and the stem was identified as either alive or dead at the end of the census interval.

Mortality was modelled in four ways:

1. **A size- and growth-independent stem mortality rate**, where all stems have equal probability of mortality:

$$M = \frac{\ln(n_0) - \ln(n_0 - n_d)}{t} \quad [1]$$

where M is the mortality rate ($year^{-1}$), n_0 is the number of stems at the start of the census interval, n_d is the number of stems that die in the census interval, and t is the mean census interval length (Lewis et al. 2004).

2. **A size-dependent stem mortality function**:

$$M(D) = ae^{b(D)}D^c \quad [2]$$

where $M(D)$ is the mortality rate ($year^{-1}$), D is the last recorded DBH of the stem, and a, b and c are plot-specific parameters fitted using maximum likelihood method (Kohyama et al. 2015) (Figure S2). The shape of this function is variable and allows mortality to vary with stem DBH in different ways.

3. **A growth-dependent stem mortality function**:

$$M(g) = \begin{cases} a\exp^{-b(g)} + c \; if \; g \; in \; (0,1) mm\, yr^{-1} \\ \dfrac{\ln(n_0) - \ln(n_0 - n_d)}{t} \; if \; g > 1 \quad mm\, yr^{-1} \end{cases} \quad [3]$$

where $M(g)$ is the mortality rate ($year^{-1}$), g is the mean annual growth rate of the stem in the previous census, and a, b and c are plot-specific parameters fitted using maximum likelihood methods (Camac et al., 2018) (Figure S3). Mortality probability is highest where g approaches zero, and declines exponentially as g increases. We fit this function for stems with annual growth rates 0–1 mm/yr, and fit a constant stem mortality rate (Eq. 1) for stems with annual growth rates > 1 mm/yr.

4. **A combination of a growth-dependent mortality function and a size-dependent mortality function**, where, at each annual growth step, the higher mortality rate estimated using Eq. 2. and 3. was selected.

Within each census interval there are some trees which recruit and die without being measured in either census, meaning that some mortality is not recorded. This is more significant in longer census intervals, and as census interval lengths increase, the true mortality rate will increasingly be underestimated (Lewis et al., 2004; Kohyama et al., 2018). We account for this by using an empirically derived correction of $Mt^{0.08}$ where M is the mortality rate estimate, and t is the mean census interval length (Lewis et al., 2004). This correction is not specific to our dataset, however it offers an approximation to account for the biases in mortality estimates introduced by the long census intervals within our dataset (Kohyama et al. 2018). We apply this correction to all mortality rate estimates, using the mean census interval length for each bioclimatic domain.

Mortality is applied at each growth step in each trajectory, and the trajectory either ends (the stem is killed) or continues to the next growth

Workflow for sampling individual growth trajectories

(A) Initialising the growth trajectory

Each trajectory begins with a stem sampled from a subset of recruits within the plot inventory data.
Each recruit has three observed state variables.

DBH_i , the first DBH measurement of the recruit	G_1 - G_{10} , the first 10 years of annual growth increments of the recruit	**WD**, the wood density of the recruit

This comprises the first 10 years of the simulated trajectory.
Growth increment data may be taken from multiple census intervals to reach 10 years.

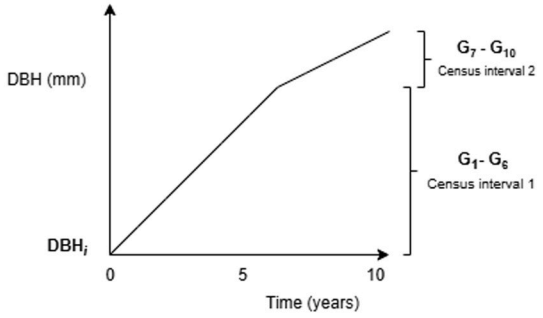

(B) Building the growth trajectory

Then new annual growth increments are randomly sampled from the full dataset.
All entries in the full dataset have five observed state variables.

$DBH_{(obs)}$, the observed DBH of the stem	$G_{(obs)}$, the observed annual growth rate of the stem in the current census interval	$G_{prev(obs)}$, the observed annual growth rate of the stem in the previous census interval	$WD_{(obs)}$, the wood density of the stem	**c**, the length of the current census interval (years)

At each sampling step, three variables describing the simulated stem are derived.

$DBH_{t(sim)}$, the DBH of the simulated stem at time *t*	$G_{prev(sim)}$, the mean annual growth rate of the simulated stem over the previous 10 years	$WD_{(sim)}$, the wood density of the simulated stem

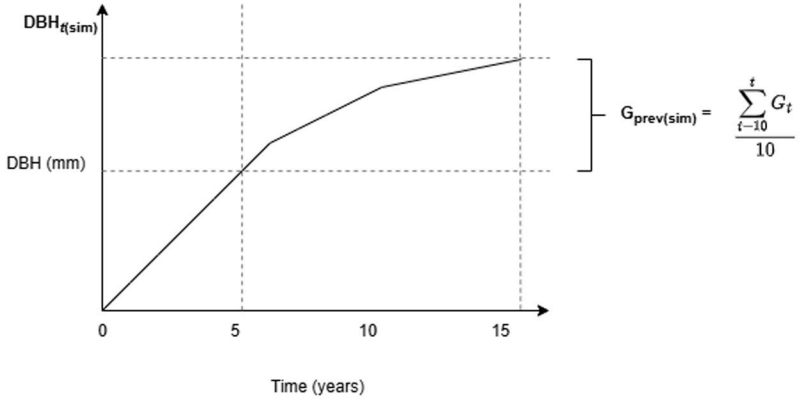

A subset of the observed dataset is generated where:

$DBH_{t(sim)}$ - 0.01 x $DBH_{t(sim)}$ > $DBH_{(obs)}$ < $DBH_{t(sim)}$ + 0.01 x $DBH_{t(sim)}$

$G_{prev(sim)}$ - 0.25 mm/year > $G_{prev(obs)}$ < $G_{prev(sim)}$ + 0.25 mm/year

$WD_{(obs)}$ = $WD_{(sim)}$

→ One stem is randomly selected, and annual growth increments $G_{(obs)}$ are added to the trajectory **c** times

→ The probability of mortality is calculated annually, and if the stem is killed, the trajectory ends

Fig. 1. Schematic to show method for building trajectories.

step (the stem survives) according to the probability of mortality. Trajectories continued until stems were killed by the mortality function. Sets of 5000 trajectories, with each trajectory representing the growth of an individual stem from 91 mm DBH to death, were generated for each bioclimatic domain and each mortality function.

2.2.3. Forest structure simulations

We simulated the structure of a typical stand for each bioclimatic domain, by randomly sampling a cohort of 100 simulated trajectories (with mortality already applied) from the full set each year, and "recruiting" them into the stand (Figure S4). As our aim is to simulate size and age structures for stands at equilibrium, recruitment is constant and not spatially explicit. Sampling of trajectories was repeated each year for 300 years to ensure that all of the stems initially recruited in year 1 had died and the stand had reached steady state.

We calculated the following structural metrics from the DBH of all stems alive at year 300: mean, median, 75% quantile, and maximum DBH, as well as the shape and scale parameters of the distribution based on a Weibull distribution fit. Higher scale parameters indicate a relatively higher proportion of large stems; the shape parameter describes the skewness of the distribution, and lower shape parameters indicate an increasingly right-skewed distribution. We also estimated simulated basal area (BA) per hectare. Because the simulation is not spatially explicit, we estimated the number of hectares represented by each simulation, based on the ratio of the number of stems at year 300 in our simulation and the mean number of stems per hectare for each bioclimatic region in the inventory data. Total BA at year 300 was then divided by this estimate of the number of hectares simulated, to estimate BA per hectare.

We also calculated metrics that summarise the age and growth rate distributions of the stand. We calculated the age of each stem as the number of years since the trajectory was initialized and calculated the mean, maximum, 75% and 90% quantiles of the age distribution of the simulated stand. Finally, we calculated the mean of the distribution of the lifetime annual growth rates of the simulated stand. Each stand-level simulation was run 100 times to estimate 95% confidence intervals of the mean for all metrics.

2.3. Validations of individual growth trajectories and simulated stand structure

2.3.1. Validation of stem diameter growth trajectories

To determine the best method for simulating multi-species growth trajectories, for each bioclimatic domain we compared the ability of each sampling approach to simulate the spread of observed tree ring trajectories. Domain-specific growth-dependent mortality models were applied to the trajectories, as detailed in Section 2.2.2, to ensure comparability with the observed tree ring trajectories. We assessed the ability of each sampling approach to simulate the distribution of ages across stems of set sizes and the distribution of sizes across stems of set ages. We used Kolmogorov-Smirnov tests to assess any significant differences between the simulated and observed size distributions at 16 different ages, and age distributions at 16 different DBH values, for each bioclimatic domain, and ranked the approaches based on the number of distributions with no significant differences between observed and simulated data. Where the distributions were significantly different, we used the Kolmogorov-Smirnov test statistic as a measure of difference to determine which approach generated the simulations with the greatest similarity to the observed data.

2.3.2. Validation of simulated stand structure

To assess the ability of the full simulation to model stand and age structure, we validated simulation outputs against observed plot census and tree ring data. We used two different simulations to compare simulated and observed data. Firstly, to compare simulated and observed stand structure, we conducted simulations using all data from all species and plots for each bioclimatic domain. For this simulation, we compared different methods of modelling mortality to determine which method produced simulations with the greatest similarity to the observed data. We compared simulated structural metrics for each bioclimatic domain with aggregated plot inventory data, selecting the most recent census of each plot between 2009 and 2018. If no censuses were available for the plot within these dates, the plot was excluded.

Secondly, to compare simulated and observed forest age structures and growth rates obtained from tree ring data, we carried out simulations using only data from the species represented within the tree ring dataset. We used only the growth-dependent mortality function in the simulations, as this function performed best in simulating size structures. We compared simulated age and growth rate metrics against the tree ring data. To ensure comparability, within the tree ring sample, we estimated individual tree ages as the number of years since stems reached 91 mm DBH, and lifetime growth rates as all annual growth rates since stems reached 91 mm DBH, as this was the size at which simulations began.

2.4. Sensitivity analyses

The Quebec provincial forest inventory dataset is an extremely well-sampled inventory dataset, with good coverage over large regions. However, many inventory datasets are sampled over smaller areas or shorter time periods. To provide guidance on the application of this approach to other inventory datasets, we ran three additional analyses. First, we ran the simulation with a range of sample sizes of recruits and different lengths of time to maturity; secondly, we ran the simulation using data from only 3 censuses for a range of sample areas (Appendix B); and thirdly, we ran the simulation for one ecological sub-region within each bioclimatic domain (Appendix C).

3. Results

3.1. Validation of trajectory simulations against tree ring data

The best-performing method for simulating trajectories involved sampling growth increments based on growth autocorrelation, diameter-dependent growth, and wood density-dependent growth, for which 88% of the simulated age and size distributions were not significantly different from the observed distributions (KS-test $p > 0.05$; Figs. 2 and S8–11; Tables S2–3). Sampling based on growth autocorrelation alone was also effective in simulating the spread of trajectories, again with 88% of the simulated age and size distributions. not significantly different from observed distributions (KS-test $p > 0.05$). However, in cases where simulated distributions differed significantly from observed distributions, the inclusion of growth autocorrelation, diameter-dependent growth, and wood density-dependent growth produced simulated distributions more similar to the observed distributions than those obtained using growth autocorrelation alone (Tables S2–3). As a result, we adopted a simulation approach that incorporated growth autocorrelation, diameter-dependent growth, and wood density-dependent growth.

Without diameter-dependent growth, growth autocorrelation, or wood density-dependent growth, the "basic" simulated trajectories tended to converge toward a similar mean growth rate, and only 30% of the simulated age and DBH distributions were similar to the observed distributions (Figs. 2 and S8–10; compare "basic" with the other approaches). Sampling based solely on diameter-dependent growth or wood density-dependent growth resulted in only modest improvement over the basic sampling framework: 34% and 41% of the simulated distributions, respectively, were similar to the observed distributions.

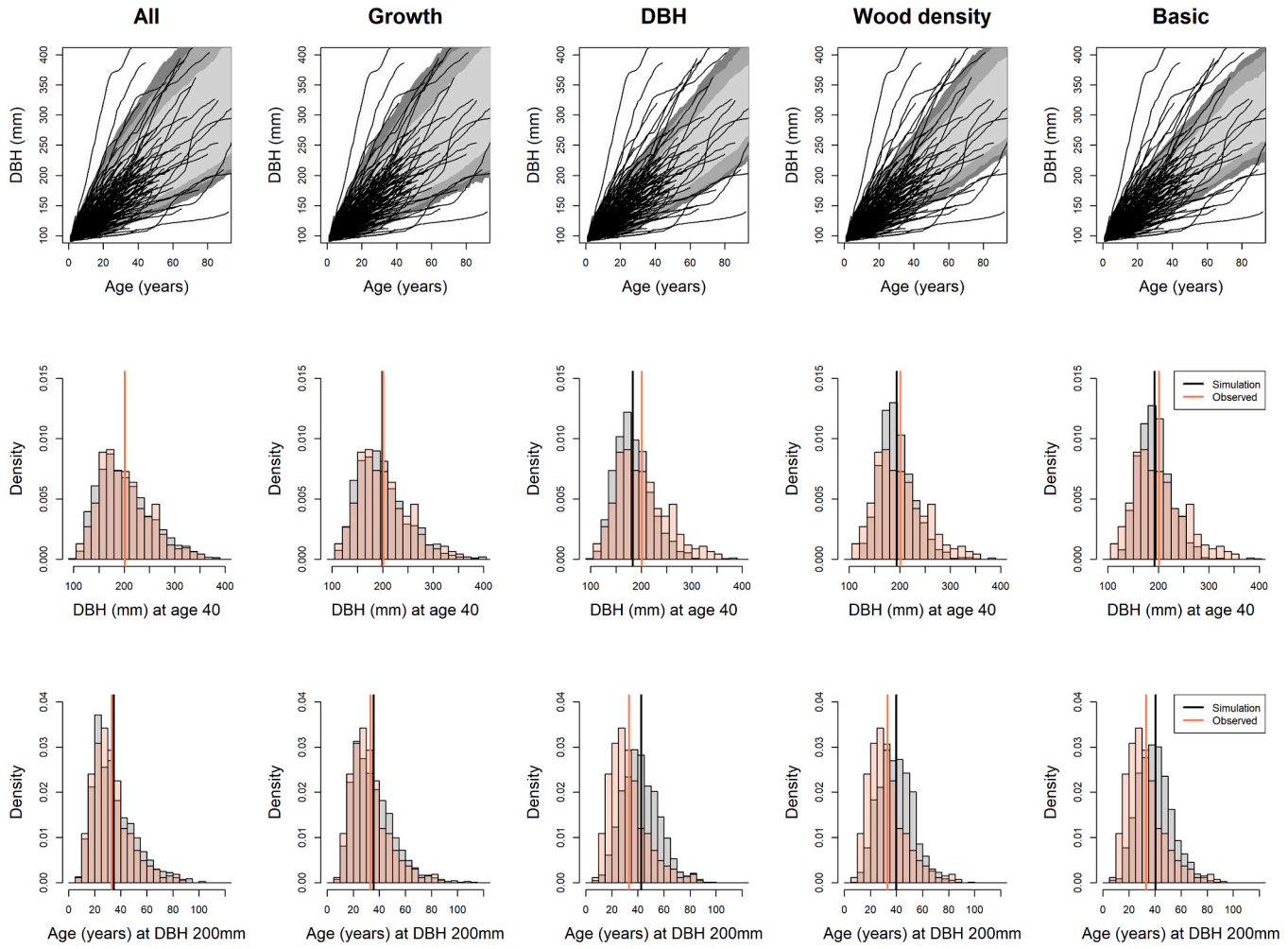

Fig. 2. Illustration of the spread of simulated trajectories under different sampling methods for the sugar maple-yellow birch domain, compared against observed tree ring trajectories. Column headings indicate whether sampling was done based on all three criteria of previous growth rate, stem DBH, and wood density, one of the criteria, or none. Row 1: variation in the spread of trajectories under different sampling frames. From light to dark, shaded grey areas show the 75%, 90% and 95% quantiles of simulated trajectories, while black lines show a sample of 300 observed tree ring trajectories. Row 2: histograms to compare the spread of simulated (grey) and observed (red) stem sizes across stems with age of 40 years since 91 mm. Vertical lines show the mean stem size for each distribution. Row 3: histograms to compare the spread of simulated (grey) and observed (red) stem ages (since 91 mm) across stems with DBH of 200 mm. Vertical lines show the mean stem age for each distribution. Simulations which successfully replicate tree ring trajectories should show a similar distribution across the full range of stem sizes or ages. Figures for the other bioclimatic domains are presented in the SI.

3.2. *Validation of simulated stand size and age structures*

3.2.1. *Validation of simulated size structure against plot inventory data*

We found that our approach to simulating stand structure, based on sampling individual tree growth trajectories, was able to generate size distributions closely matching the observed distributions, although performance varied strongly with the mortality function that was used. Simulations employing the growth-dependent mortality function produced structural metrics most similar to those observed. Across all four bioclimatic domains, simulations using this mortality function estimated 20 out of 24 structural metrics within 10% of observed values, and all metrics within 20% (Table 2). In contrast, simulations using the alternative mortality functions significantly underestimated maximum DBH, the scale parameter, and BA, with estimation errors exceeding 20% (Table 2). These results suggest that those functions overestimated mortality rates of the largest stems, thereby failing to accurately simulate large-stem frequencies.

3.2.2. *Validation of simulated age structure and growth rates against tree ring data*

This approach also generated realistic simulations of stand age and growth rate distributions (Fig. 3). Across all bioclimatic domains, simulated estimates of mean stem age and the 75% and 90% quantiles of the stem age distribution were comparable to those derived from the tree ring data (Fig. 3; Table 3). Simulated estimates of maximum stand age were less accurate, likely due in part to the rarity of very old stems, which makes this metric sensitive to the small sample size of the tree ring data. Simulated estimates of mean annual growth rate were within + /- 8% of the mean annual growth rate calculated from the tree ring sample (Table 3).

3.3. *Sensitivity analyses*

The sensitivity analyses showed that our approach can also be applied to simulate stand-level metrics across smaller sample areas (Appendix B), and at the sub-regional level (Appendix C). We find that simulated size and age structures are highly variable where the area sampled is < 2 ha but stabilize as the sample area increases. Our results indicate that, at least within these bioclimatic domains, a minimum sample area of 10 ha is sufficient to produce stable simulations, though we expect that a higher sample area will be required in more diverse forests (Appendix B). In contrast, in less diverse regions, such as the

Table 2
Mean percentage differences between observed and simulated stand structure variables, for each bioclimatic domain and each method of modelling mortality. From the domain-level simulated stand structure, we calculated summary structural variables, and compared these to summary variables calculated from the plot inventory data, aggregated at the domain level. Cells are coloured to indicate the percentage difference between each simulated value and the observed value, where green cells show simulations within 10% of the observed value, yellow cells between 10% and 20% of the observed value, and orange cells over 20% difference from the observed value.

Bioclimatic domain	Mortality function	Mean DBH	Median DBH	75% quantile DBH	Basal area	Scale parameter	Shape parameter	Maximum DBH
Sugar maple-yellow birch	Growth dependent mortality	1	2	2	2	0	0	-4
	Size dependent mortality	-8	-3	-6	-23	-15	4	-15
	Growth and size dependent mortality	-7	-2	-4	-22	-13	5	-15
	Constant mortality	-13	-10	-15	-30	-28	2	-25
Balsam fir-yellow birch	Growth dependent mortality	5	2	6	9	7	-4	7
	Size dependent mortality	-2	-4	-1	-7	-9	-7	-2
	Growth and size dependent mortality	-2	-4	-2	-9	-10	-6	-4
	Constant mortality	-8	-7	-9	-18	-21	-3	-50
Balsam fir-white birch	Growth dependent mortality	6	1	5	15	9	-9	17
	Size dependent mortality	-4	-4	-4	-12	-13	-3	-5
	Growth and size dependent mortality	-4	-4	-4	-13	-15	-3	-7
	Constant mortality	-6	-7	-8	-13	-21	-7	-29
Spruce-moss	Growth dependent mortality	1	-4	-1	9	-6	-18	12
	Size dependent mortality	-9	-10	-12	-18	-30	-11	-12
	Growth and size dependent mortality	-9	-10	-12	-19	-32	-10	-13
	Constant mortality	-9	-11	-12	-20	-34	-15	-40

balsam fir-white birch and spruce-moss domains, we generated accurate simulations of stand structure using only ~7 ha sample area (Appendix C). Estimates of stand size and age structure are robust to variation in recruitment sample size and time to maturity (Figures S5–6).

4. Discussion

Our results show that stem growth trajectories can be modelled using repeated sampling of annual growth increments taken from plot inventory data. This is the first time that this approach to simulating growth trajectories has been applied to repeat plot inventory data and validated using separate datasets to build (using multi-census plot data) and validate (using tree ring data) the trajectories (see Brienen et al. 2006 for modelling and validation with a single dataset). We found that inclusion of growth autocorrelation in the approach created a realistic spread of trajectories, while inclusion of diameter-dependent growth and wood density-dependent growth had a smaller effect. These results suggest that, where wood density data is unavailable, growth autocorrelation alone may be sufficient to simulate trajectories with reasonable accuracy. As wood density correlates negatively with growth rate (Chave et al., 2005), inclusion of growth autocorrelation may already account for much of the wood density-dependent variation in growth, reducing the effect of including wood density. However, species diversity in this dataset is relatively low; even in the most diverse domain (sugar maple-yellow birch), just 3 species account for 65% of all stems and there is significant overlap in the growth rate distributions among species (Figure S12), meaning that within-species variation in growth rate may be just as important in determining the spread of trajectories as between-species variation in growth rate. The importance of wood density and species identity in shaping stand-level variation in growth rates might increase in more diverse forests.

Simulated growth trajectories are a valuable tool to estimate stand and species age distributions, and the approach could be further developed to estimate stand tree turnover, which is an important predictor of forest biomass (Körner, 2017). This would be particularly useful in the tropics, where ring formation is rare, and estimation of species ages and longevities is challenging (Baker, 2003; Brienen et al., 2016; Vieira et al., 2005), although further validation may be required to assess the reliability of this approach in forests with higher species diversity.

Our approach to simulating full stand structure, based on repeated sampling of growth trajectories, accurately captured the observed latitudinal variation in stand structure, age, and growth rates in forests in Quebec. Mean DBH and the relative proportion of large stems decline

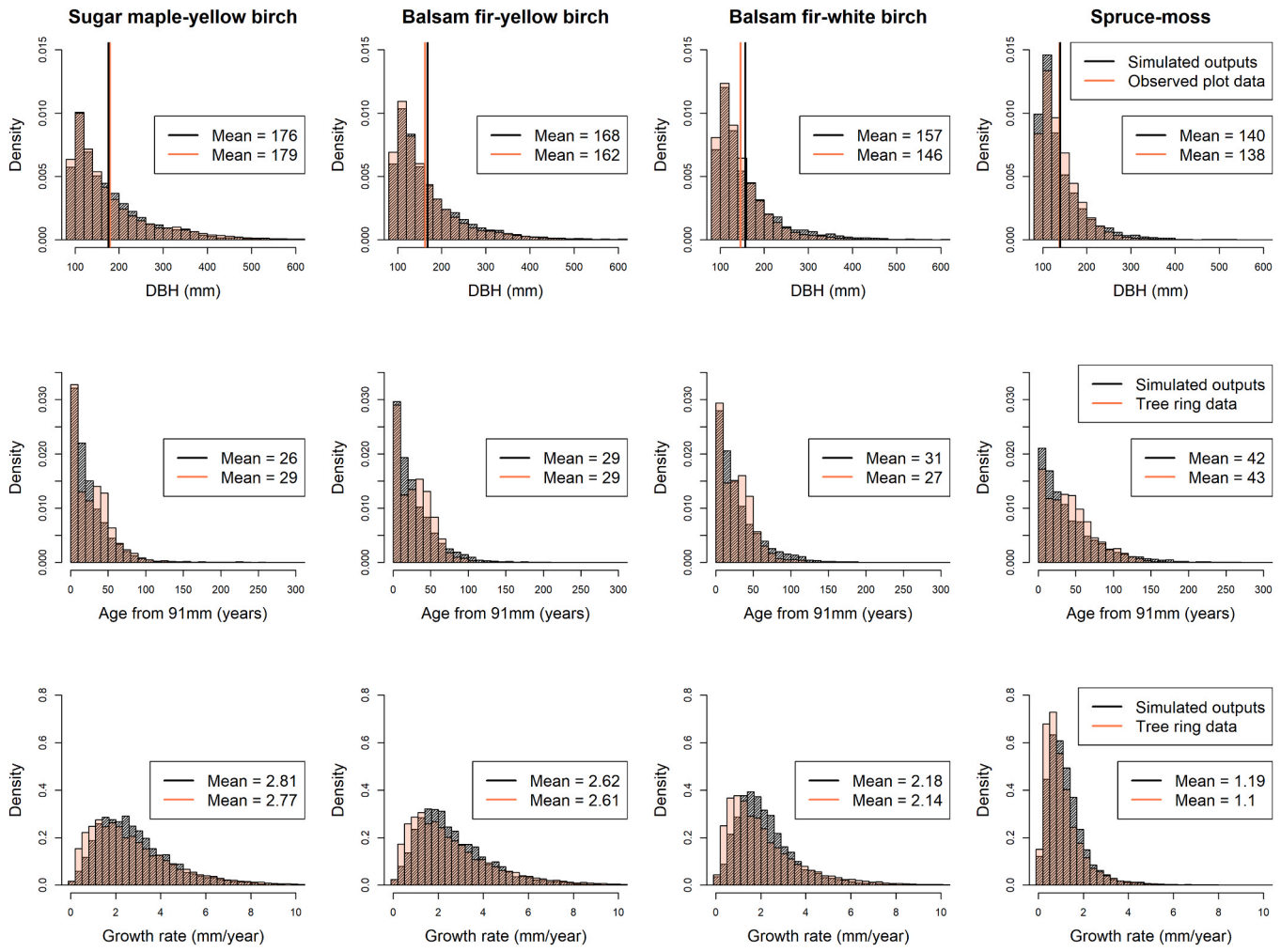

Fig. 3. Histograms comparing observed stand size and age structures, and growth rate distributions with simulation outputs using the growth-dependent mortality function. Row 1: comparisons of stem size distributions of typical stands generated from simulated stem growth trajectories (black hatched) and observed forest structure from plot census data for each bioclimatic domain (red). Row 2: comparisons of age distributions of typical stands generated from simulated stem growth trajectories (black hatched) and observed age distributions from the tree ring data (red), for each bioclimatic domain. Row 3: comparisons of growth rate distributions of typical stands generated from simulated stem growth trajectories (black hatched) and observed growth rate distributions from the tree ring data, for each bioclimatic domain.

Table 3
Comparisons of growth rate and age distribution statistics between simulated stands and the tree ring sample, for each bioclimatic domain. All ages are from when the stem first reached 91 mm DBH. The range of simulated metrics is shown in brackets.

		Mean annual growth rate ($mmyr^{-1}$)	Mean stem age (years)	75% quantile stem age (years)	90% quantile stem age (years)	Maximum stem age (years)
Sugar maple-yellow birch	Simulated output	2.74 (2.66, 2.80)	25.7 (24.6, 26.7)	35 (33, 37)	58 (55, 62)	222 (164, 246)
	Tree ring sample	2.77	29	43	60	210
Balsam fir-yellow birch	Simulated output	2.70 (2.65, 2.77)	28.7 (27.3, 30.3)	40 (38, 42)	66 (61, 69)	192 (168, 212)
	Tree ring sample	2.61	29	43	59	158
Balsam fir-white birch	Simulated output	2.11 (2.04, 2.15)	29.8 (28.8, 30.7)	41 (40, 43)	67 (64, 70)	198 (173, 216)
	Tree ring sample	2.14	27	40	55	176
Spruce-moss	Simulated output	1.18 (1.16, 1.21)	42.2 (40.9, 43.3)	58 (56, 60)	96 (91, 101)	292 (271, 300)
	Tree ring sample	1.10	43	60	88	194

with increasing latitude, which is likely associated with the higher mean growth rates and higher frequencies of fast-growing stems in the lower latitude domains (Fig. 3; Duchesne et al., 2019). In the two temperate domains mortality rates are higher and mean stand age is lower (Table 1), indicating higher stem turnover rates, while stems in the boreal spruce-moss domain are slow-growing but longer-lived. This model has strong potential to be developed further to answer questions about the relative importance of growth, mortality, and turnover controls on stand structure.

Our results also highlight the importance of demographic rates in determining forest structure: across the four bioclimatic domains, variation in forest structure can be described almost entirely using data on growth and mortality. Importantly, only limited information on species identity, as it relates to wood density, is required for accurate simulation. This success is likely attributable firstly to the strong effect of growth autocorrelation and the close association between growth rates and species functional traits. Plant functional traits clearly differentiate species along a fast-slow trait spectrum and are strongly correlated with variation in demographic rates (Reich, 2014; Rüger et al., 2020), meaning that information on species traits and composition is inherent in the sample of growth increments measured in plot census data. By employing growth autocorrelation, the sampling approach automatically samples growth increments from individuals with similar functional traits, which may reduce the need to explicitly account for a range of traits. Rüger et al. (2020), showed that grouping species into 5 plant functional clusters across two axes of variation (a growth-survival trade-off and a stature-recruitment trade-off) was sufficient to accurately model stand structure in a tropical forest. Our results suggest that, at least for boreal forests, even simpler approaches may be sufficient. Secondly, the results likely reflect the strong association between wood density and growth rates, whereby sampling frames based on wood density induce long-term variation in growth (i.e. large divergence of size-age trajectories). Re-sampling growth increments based on wood density offers a way to sample representative growth rates in more diverse datasets, where there may be either insufficient growth increment measurements from each species, or individuals that are identified only to the level of family or genus.

The results also point to the importance of mortality in determining forest structure. We find that simulation outputs vary strongly according to the mortality function that is used, particularly for estimates of stand age, growth rate, and BA. In Quebec, fitted mortality functions depended strongly on growth, and only weakly on size. The strikingly high mortality rates of individuals with low growth rates (up to ~20% annual mortality for stems showing no growth in the previous year) indicate that growth rate is the best predictor of mortality in these forests, and that drivers of mortality, such as physiological stress, are strongly associated with low growth rates. A strong influence of growth-dependent mortality in shaping forest dynamics, structure, and composition has been observed in other temperate and high-latitude forests (Cailleret et al., 2016; Kobe, 1996). However, a growth-dependent mortality function may not be the best fit to other datasets, as the relative influence of different modes of mortality varies strongly with forest type and age (Cailleret et al., 2020; Larson et al., 2015; Needham et al., 2020). For example, strong size-dependency of mortality has previously been identified in tropical forests (Gora and Esquivel-Muelbert, 2021), suggesting that case-by-case determination of an appropriate mortality function will be important for wider application of this approach.

While our approach is simple, it offers a foundation for more detailed modelling of forest dynamics. Unlike many individual-based models, which may require trait or spatial data, the approach simulates stand structure using only basic forest inventory data, and so in principle has the potential to be applied easily to other forest inventory datasets, albeit with some important caveats. Here, we have assessed our approach within natural forests with a small range of species; however most other inventory datasets will be from more diverse forests, particularly in the tropics, which is likely to add additional complexity. Firstly, the range of life-history strategies and growth rates is much higher in tropical and sub-tropical regions (Bialic-Murphy et al., 2024; Needham et al., 2022), and so simulation of realistic growth trajectories may require growth increments to be selected based on a wider range of functional traits. Similarly, use of a single plot-level mortality function may be insufficient to accurately model mortality in stands where high species and life history diversity may mask any strong stand-level size- or growth-dependencies. Instead mortality functions may have to be parameterized according to functional group or canopy status (Johnson et al., 2018). We would advocate for local drivers of growth and mortality to be considered when adapting this approach to new sites, and for careful assessment of outputs at steady state before using the simulation for projections.

One further limitation of the simulation approach is that information on recruitment is not included, and as a result the model outputs are not spatially explicit. While it is possible to obtain a "per area" estimate of BA and AGB through comparison of the number of trees in the simulation (once equilibrium is reached) and the observed tree density of the plot data, direct inclusion of site-specific recruitment data would allow for the simulation of stand-level properties, and a more intuitive interpretation of outputs. Furthermore, the lack of recruitment means that it is not currently possible to model recruitment responses to, for example, increased mortality and disturbance. Future development of the approach should therefore focus on inclusion of recruitment data.

We expect that wider application of this method should enable studies of forest dynamics and demographic controls on forest structure spatially and temporally. For example, once the model is parameterized to simulate stands under demographic equilibrium, mortality and growth can be varied through time in order to simulate structure under non-equilibrium conditions, such as with climate- or disturbance-driven increases in mortality rate. Because there are no inbuilt assumptions about growth responses to changes in competition, resource availability, or climate, outputs can provide "null" baseline expectations of forest structural responses under different scenarios of demographic change. This is valuable for assessing how growth longevity trade-offs combined with increases in growth could explain apparent global increases in mortality (Brienen et al., 2020; Yu et al., 2019), or exploring how growth stimulation may be driving global shifts in forest size distributions (Marqués et al., 2023; Esquivel-Muelbert et al., 2025).

CRediT authorship contribution statement

Louis Duchesne: Writing – review & editing, Data curation. **Timothy Baker:** Writing – review & editing, Project administration, Conceptualization. **Roel Brienen:** Writing – review & editing, Project administration, Conceptualization. **Gloor Emanuel:** Writing – review & editing, Project administration, Conceptualization. **Rebecca Banbury Morgan:** Writing – review & editing, Writing – original draft, Visualization, Formal analysis, Data curation, Conceptualization.

Funding

R.B.M. was funded by the NERC Panorama Doctoral Training Partnership (NE/S007458/1).

Declaration of Competing Interest

The authors have no competing interests to declare.

Acknowledgements

We wish to thank the staff of the *Direction des inventaires forestiers* of the *Ministère des Ressources naturelles et des Forêts* (MRNF) of Quebec Government, for their work relating to the forest inventory program, and for sharing with us the tree-ring and sample plot data.

Appendix A. Supporting information

Supplementary data associated with this article can be found in the online version at doi:10.1016/j.foreco.2026.123704.

Data availability

Full code, documentation and sample data needed to run the simulation, alongside example trajectories, are available in the Zenodo repository at 10.5281/zenodo.19183014. Data from the Quebec provincial forest inventory program permanent sample plots is publicly available and can be downloaded from the following site: https://www.donneesquebec.ca/recherche/fr/dataset/placettes-echantillons-permanentes-1970-a-aujourd-hui. Tree ring data can be obtained on request from the *Direction des inventaires forestiers* of the *Ministère des Ressources naturelles et des Forêts du Québec*.

References

Anderson-Teixeira, K.J., Davies, S.J., Bennett, A.C., Gonzalez-Akre, E.B., Muller-Landau, H.C., Joseph Wright, S., Abu Salim, K., Almeyda Zambrano, A.M., Alonso, A., Baltzer, J.L., Basset, Y., Bourg, N.A., Zimmerman, J., 2015. CTFS-ForestGEO: a worldwide network monitoring forests in an era of global change. Glob. Change Biol. 21, 528–549. https://doi.org/10.1111/gcb.12712.

Anderson-Teixeira, K.J., Herrmann, V., Rollinson, C.R., Gonzalez, B., Gonzalez-Akre, E. B., Pederson, N., Alexander, M.R., Allen, C.D., Alfaro-Sánchez, R., Awada, T., Baltzer, J.L., Baker, P.J., Zuidema, P.A., 2022. Joint effects of climate, tree size, and year on annual tree growth derived from tree-ring records of ten globally distributed forests. Glob. Change Biol. 28 (1), 245–266. https://doi.org/10.1111/gcb.15934.

Baker, P.J., 2003. Tree age estimation for the tropics: A test from the southern Appalachians. Ecol. Appl. 13 (6), 1718–1732. https://doi.org/10.1890/02-5025.

Baraloto, C., Rabaud, S., Molto, Q., Blanc, L., Fortunel, C., Hérault, B., Dávila, N., Mesones, I., Rios, M., Valderrama, E., Fine, P.V.A., 2011. Disentangling stand and environmental correlates of aboveground biomass in Amazonian forests. Glob. Change Biol. 17 (8), 2677–2688. https://doi.org/10.1111/j.1365-2486.2011.02432.x.

Bialic-Murphy, L., McElderry, R.M., Esquivel-Muelbert, A., Van Den Hoogen, J., Zuidema, P.A., Phillips, O.L., Almeida de Oliveira, E., Alvarez Loayza, P., Alvarez-Davila, E., Alves, L.F., Andrade Maia, V., Crowther, T.W., 2024. The pace of life for forest trees. Science 386, 92–98. https://doi.org/10.1126/science.adk9616.

Brienen, R.J.W., Zuidema, P.A., During, H.J., 2006. Autocorrelated growth of tropical forest trees: Unraveling patterns and quantifying consequences. For. Ecol. Manag. 237 (1-3), 179–190. https://doi.org/10.1016/j.foreco.2006.09.042.

Brienen, R.J.W., Gloor, E., Zuidema, P.A., 2012. Detecting evidence for CO_2 fertilization from tree ring studies: The potential role of sampling biases. Glob. Biogeochem. Cycles 26 (1). https://doi.org/10.1029/2011GB004143.

Brienen, R.J.W., Schöngart, J., Zuidema, P.A., 2016. In: Goldstein, G., Santiago, L.S. (Eds.), Tree Rings in the Tropics: Insights into the Ecology and Climate Sensitivity of Tropical Trees BT - Tropical Tree Physiology: Adaptations and Responses in a Changing Environment. Springer International Publishing, pp. 439–461. https://doi.org/10.1007/978-3-319-27422-5_20.

Brienen, R.J.W., Caldwell, L., Duchesne, L., Voelker, S., Barichivich, J., Baliva, M., Ceccantini, G., Di Filippo, A., Helama, S., Locosselli, G.M., Lopez, L., Piovesan, G., Schöngart, J., Villalba, R., Gloor, E., 2020. Forest carbon sink neutralized by pervasive growth-lifespan trade-offs. Nat. Commun. 11 (1), 1–10.

Cailleret, M., Jansen, S., Robert, E.M.R., Janda, P., Kane, J.M., Kharuk, V.I., Tognetti, R., 2016. A synthesis of radial growth patterns preceding tree mortality. & Jos E 1–16. https://doi.org/10.1111/gcb.13535.

Cailleret, M., Bircher, N., Hartig, F., Hülsmann, L., Bugmann, H., 2020. Bayesian calibration of a growth-dependent tree mortality model to simulate the dynamics of European temperate forests. Ecol. Appl. 30 (1). https://doi.org/10.1002/eap.2021.

Camac, J.S., Condit, R., FitzJohn, R.G., McCalman, L., Steinberg, D., Westoby, M., Wright, S.J., Falster, D.S., 2018. Partitioning mortality into growth-dependent and growth-independent hazards across 203 tropical tree species. Proc. Natl. Acad. Sci. U.S.A. 115 (49), 12459–12464. https://doi.org/10.1073/pnas.1721040115.

Caspersen, J.P., Vanderwel, M.C., Cole, W.G., Purves, D.W., 2011. How stand productivity results from size- and competition-dependent growth and mortality. PLoS ONE 6 (12). https://doi.org/10.1371/journal.pone.0028660.

Chave, J., 1999. Study of structural, successional and spatial patterns in tropical rain forests using TROLL, a spatially explicit forest model. Ecol. Model. 124 (2-3), 233–254. https://doi.org/10.1016/S0304-3800(99)00171-4.

Chave, J., Andalo, C., Brown, S., Cairns, M.A., Chambers, J.Q., Eamus, D., Fölster, H., Fromard, F., Higuchi, N., Kira, T., Lescure, J.P., Nelson, B.W., Ogawa, H., Puig, H., Riéra, B., Yamakura, T., 2005. Tree allometry and improved estimation of carbon stocks and balance in tropical forests. Oecologia 145 (1), 87–99. https://doi.org/10.1007/s00442-005-0100-x.

Chave, J., Coomes, D., Jansen, S., Lewis, S.L., Swenson, N., Zanne, A.E., 2009. Towards a worldwide wood economics spectrum. Ecol. Lett. 12 (4), 351–366. https://doi.org/10.1111/j.1461-0248.2009.01285.x.

Coomes, D.A., Allen, R.B., 2007. Mortality and Tree-Size Distributions in Natural Mixed-Age Forests, 95 (1), 27–40.

Cruz, M., Lieberman, D., Lieberman, M., 2020. Tropical tree growth and longevity: Validation of Growth Simulation, a bootstrapping model. J. Sustain. For. 39 (7), 674–691.

Duchesne, L., Houle, D., Ouimet, R., Caldwell, L., Gloor, M., Brienen, R., 2019. Large apparent growth increases in boreal forests inferred from tree-rings are an artefact of sampling biases. Sci. Rep. 9, 6832. https://doi.org/10.1038/s41598-019-43243-1.

Esquivel-Muelbert, A., Banbury Morgan, R., Brienen, R., et al., 2025. Increasing tree size across Amazonia. Nat. Plants 11, 2016–2025. https://doi.org/10.1038/s41477-025-02097-4.

Fischer, R., Bohn, F., Dantas de Paula, M., Dislich, C., Groeneveld, J., Gutiérrez, A.G., Kazmierczak, M., Knapp, N., Lehmann, S., Paulick, S., Pütz, S., Rödig, E., Taubert, F., Köhler, P., Huth, A., 2016. Lessons learned from applying a forest gap model to understand ecosystem and carbon dynamics of complex tropical forests. Ecol. Model. 326, 124–133. https://doi.org/10.1016/j.ecolmodel.2015.11.018.

ForestPlots.net, Blundo, C., Carilla, J., Grau, R., Malizia, A., Malizia, L., Osinaga-Acosta, O., Bird, M., Bradford, M., Catchpole, D., Ford, A., Graham, A., Hilbert, D., Kemp, J., Laurance, S., Laurance, W., Tran, H.D., 2021. Taking the pulse of Earth's tropical forests using networks of highly distributed plots. Biol. Conserv. 260 (May). https://doi.org/10.1016/j.biocon.2020.108849.

Fortin, M., Langevin, L., 2012. Stochastic or deterministic single-tree models: is there any difference in growth predictions? Ann. For. Sci. 69, 271–282. https://doi.org/10.1007/s13595-011-0112-0.

Fortin, M., Bédard, S., DeBlois, J., Meunier, S., 2009. Assessing and testing prediction uncertainty for single tree-based models: A case study applied to northern hardwood stands in southern Québec, Canada. Ecol. Model. 220, 2770–2781. https://doi.org/10.1016/j.ecolmodel.2009.06.035.

Friedlingstein, P., O'Sullivan, M., Jones, M.W., Andrew, R.M., Gregor, L., Hauck, J., Le Quéré, C., Luijkx, I.T., Olsen, A., Peters, G.P., Peters, W., Pongratz, J., Schwingshackl, C., Sitch, S., Canadell, J.G., Zheng, B., 2022. Global Carbon Budget 2022. Earth Syst. Sci. Data 14, 4811–4900. https://doi.org/10.5194/essd-14-4811-2022.

Gora, E.M., Esquivel-Muelbert, A., 2021. Implications of size-dependent tree mortality for tropical forest carbon dynamics. Nat. Plants 7 (4), 384–391. https://doi.org/10.1038/s41477-021-00879-0.

Gray, A., Brandeis, T., Shaw, J., McWilliams, W., Miles, P., 2012. Forest Inventory and Analysis Database of the United States of America (FIA). Biodivers. Ecol. 4, 225–231. https://doi.org/10.7809/b-e.00079.

Hember, R.A., Kurz, W.A., 2018. Low Tree-Growth Elasticity of Forest Biomass Indicated by an Individual-Based Model. Forests 9 (1), 21. https://doi.org/10.3390/f9010021.

Johnson, D.J., Needham, J., Xu, C., Massoud, E.C., Davies, S.J., Anderson-Teixeira, K.J., Bunyavejchewin, S., Chambers, J.Q., Chang-Yang, C.H., Chiang, J.M., Chuyong, G. B., Condit, R., McMahon, S.M., 2018. Climate sensitive size-dependent survival in tropical trees. Nat. Ecol. Evol. 2 (9), 1436–1442. https://doi.org/10.1038/s41559-018-0626-z.

Kobe, R.K., 1996. Intraspecific variation in sapling mortality and growth predicts geographic variation in forest composition. Ecol. Monogr. 66 (2), 181–201.

Kohyama, T., Kubo, T., Macklin, E., 2005. Effect of temporal autocorrelation on apparent growth rate variation in forest tree census data and an alternative distribution function of tree growth rate. Ecol. Res. 20 (1), 11–15. https://doi.org/10.1007/s11284-004-0007-8.

Kohyama, T., Potts, M., Kohyama, T., Kassim, A., Ashton, P., 2015. Demographic properties shape tree size distribution in a Malaysian rain forest. Am. Nat. 185 (3), 367–379. https://doi.org/10.1086/679664.

Kohyama, T.S., Kohyama, T.I., Sheil, D., 2018. Definition and estimation of vital rates from repeated censuses: Choices, comparisons and bias corrections focusing on trees. Methods Ecol. Evol. 9, 809–821. https://doi.org/10.1111/2041-210X.12929.

Körner, C., 2017. A matter of tree longevity. Science 355 (6321), 130–131. https://doi.org/10.1126/science.aal2449.

Larson, A.J., Lutz, J.A., Donato, D.C., Freund, J.A., Swanson, M.E., HilleRisLambers, J., Sprugel, D.G., Franklin, J.F., 2015. Spatial aspects of tree mortality strongly differ between young and old-growth forests. Ecology 96 (11), 2855–2861.

Lewis, S.L., Phillips, O.L., Sheil, D., Vinceti, B., Baker, T.R., Brown, S., Graham, A.W., Higuchi, N., Hilbert, D.W., Laurance, W.F., Lejoly, J., Malhi, Y., Monteagudo, A., Vargas, P.N., Sonké, B., Nur Supardi, M.N., Terborgh, J.W., Martínez, R.V., 2004. Tropical forest tree mortality, recruitment and turnover rates: Calculation, interpretation and comparison when census intervals vary. J. Ecol. 92 (6), 929–944. https://doi.org/10.1111/j.0022-0477.2004.00923.x.

Lieberman, D., Lieberman, M., Hartshorn, G., Peralta, R., 1985. Growth rates and age-size relationships of tropical wet forest trees in Costa Rica. J. Trop. Ecol. 1 (2), 97–109.

Lieberman, M., Lieberman, D., 1985. Simulation of growth curves from periodic increment data. Ecology 66 (2), 632–635.

Marqués, L., Weng, E., Bugmann, H., Forrester, D.I., Rohner, B., Hobi, M.L., Trotsiuk, V., Stocker, B.D., 2023. Tree Growth Enhancement Drives a Persistent Biomass Gain in Unmanaged Temperate Forests. AGU Adv. 4 (5), 1–19. https://doi.org/10.1029/2022AV000859.

Ministère des Forêts, de la Faune et des Parcs (MFFP), 2014. Réseaux des placettes-échantillons permanentes du Québec méridional. Gouvernement du Québec, Ministère des Forêts. de la Faune et des Parcs, Direction des inventaires forestiers. ⟨https://mffp.gouv.qc.ca/documents/forets/inventaire/Reseaux-PEP.pdf⟩.

Ministère des Forêts, de la Faune et des Parcs (MFFP), 2016. Norme d'inventaire écoforestier, placettes-échantillons permanentes, édition 2016. Gouvernement du Québec, Ministère des Forêts. de la Faune et des Parcs, Direction des inventaires forestiers. ⟨https://mffp.gouv.qc.ca/documents/forets/inventaire/Norme-PEP.pdf⟩.

Ministère des Ressources naturelles et des Forêts (MRNF). (2022). Placette-échantillon permanente [dataset]. ⟨https://www.donneesquebec.ca/recherche/fr/dataset/placettes-echantillons-permanentes-1970-a-aujourd-hui⟩.

Muller-Landau, H.C., Condit, R.S., Harms, K.E., Marks, C.O., Thomas, S.C., Bunyavejchewin, S., Chuyong, G., Co, L., Davies, S., Foster, R., Gunatilleke, S., Gunatilleke, N., Hart, T., Hubbell, S.P., Itoh, A., Ashton, P., 2006. Comparing tropical forest tree size distributions with the predictions of metabolic ecology and equilibrium models. Ecol. Lett. 9, 589–602. https://doi.org/10.1111/j.1461-0248.2006.00915.x.

Needham, J.F., Chambers, J., Fisher, R., Knox, R., Koven, C.D., 2020. Forest responses to simulated elevated CO2 under alternate hypotheses of size- and age-dependent mortality. Glob. Change Biol. 26 (10), 5734–5753. https://doi.org/10.1111/gcb.15254.

Needham, J.F., Johnson, D.J., Anderson-Teixeira, K.J., Bourg, N., Bunyavejchewin, S., Butt, N., Cao, M., Cárdenas, D., Chang-Yang, C.-H., Chen, Y.-Y., Chuyong, G., Dattaraja, H.S., Davies, S.J., Duque, A., McMahon, S.M., 2022. Demographic composition, not demographic diversity, predicts biomass and turnover across temperate and tropical forests. Glob. Change Biol. 28 (9), 2895–2909. https://doi.org/10.1111/gcb.16100.

Pacala, S.W., Canham, C.D., Saponara, J., Silander, J.A., Kobe, R.K., Ribbens, E., 1996. Forest models defined by field measurements: estimation, error analysis and dynamics. Ecol. Monogr. 66 (1), 1–43. https://doi.org/10.2307/2963479.

Pan, Y., Birdsey, R.A., Phillips, O.L., Houghton, R.A., Fang, J., Kauppi, P.E., Keith, H., Kurz, W.A., Ito, A., Lewis, S.L., Nabuurs, G.J., Shvidenko, A., Hashimoto, S., Lerink, B., Schepaschenko, D., Castanho, A., Murdiyarso, D., 2024. The enduring world forest carbon sink. Nature 631, 563–569. https://doi.org/10.1038/s41586-024-07602-x.

Rammer, W., Thom, D., Baumann, M., Braziunas, K., Dollinger, C., Kerber, J., Mohr, J., Seidl, R., 2024. The individual-based forest landscape and disturbance model iLand: Overview, progress, and outlook. Ecol. Model. 495, 110785. https://doi.org/10.1016/j.ecolmodel.2024.110785.

Reich, P.B., 2014. The world-wide 'fast–slow ' plant economics spectrum: a traits manifesto. J. Ecol. 102 (2), 275–301. https://doi.org/10.1111/1365-2745.12211.

Rüger, N., Condit, R., Dent, D.H., DeWalt, S.J., Hubbell, S.P., Lichstein, J.W., Lopez, O.R., Wirth, C., Farrior, C.E., 2020. Demographic trade-offs predict tropical forest dynamics. Science 368 (6487), 165–168. https://doi.org/10.1126/science.aaz4797.

Vieira, S., Trumbore, S., Camargo, P.B., Selhorst, D., Chambers, J.Q., Higuchi, N., Martinelli, L.A., 2005. Slow growth rates of Amazonian trees: Consequences for carbon cycling. Proc. Natl. Acad. Sci. U. S. A. 102 (51), 18502–18507. https://doi.org/10.1073/pnas.0505966102.

Yu, K., Smith, W.K., Trugman, A.T., Condit, R., Hubbell, S.P., Sardans, J., Peng, C., Zhu, K., Peñuelas, J., Cailleret, M., Levanic, T., Gessler, A., Schaub, M., Ferretti, M., Anderegg, W.R.L., 2019. Pervasive decreases in living vegetation carbon turnover time across forest climate zones. Proc. Natl. Acad. Sci. U. S. A. 116 (49), 24662–24667. https://doi.org/10.1073/pnas.1821387116.